catalysts

MDPI

Article

Effect of Hydroxylation and Carboxylation on the Catalytic Activity of Fe_2O_3/Graphene for Oxidative Desulfurization and Denitration

Gang Lu [1], Hengyi Liao [2], Xing Zheng [2], Congkun Chen [2], Weiliang Wang [3], Xianbin Xiao [2,*] and Wu Qin [2,*]

[1] Tianjin Jinneng Binhai Thermal Power Co., Ltd., Tianjin 300450, China
[2] School of New Energy, North China Electric Power University, Beijing 102206, China
[3] Energy and Electricity Research Center, International School of Energy, Jinan University, No. 206 Qianshan Road, Zhuhai 519070, China
* Correspondence: xiaoxianbin@ncepu.edu.cn (X.X.); qinwu@ncepu.edu.cn (W.Q.)

Abstract: Iron-based particles loaded on porous carbon materials have attracted extensive attention as catalysts for denitration and desulfurization reactions. However, the carbon support of a high-temperature denitration catalyst is inevitably oxidized in the presence of H_2O and O_2. The mechanism of denitration catalyst oxidation and its influence on the catalytic reaction remain to be further explored. Fe_2O_3-loaded graphene models with carbon vacancy (G_{def}), hydroxyl (HyG), and carboxyl (CyG) were constructed to investigate the effects of hydroxylation and carboxylation on the catalytic activity of Fe_2O_3/graphene for oxidative desulfurization and denitration by using density functional theory (DFT) calculations. According to the analysis of structural properties and adsorption energy, the adsorption process of Fe_2O_3 on HyG and CyG was observed to have proceeded more favorably than that on G_{def}. The density-of-states (DOS) results also affirmed that HyG and CyG promote the electron delocalization of Fe_2O_3 around the Fermi level, enhancing the chemical activity of Fe_2O_3. Moreover, adsorption energy analysis indicates that hydroxylation and carboxylation enhanced the adsorption of SO_2 and H_2O_2 on Fe_2O_3/graphene while also maintaining preferable adsorption stability of NO. Furthermore, mechanistic research explains that adsorbed H_2O_2 on HyG and CyG directly oxidizes NO and SO_2 into HNO_2 and H_2SO_4 following a one-step reaction. The results provide a fundamental understanding of the oxidized catalyst on catalytic denitration and desulfurization reactions.

Keywords: Fe_2O_3/G_{def}; Fe_2O_3/HyG; Fe_2O_3/CyG; hydroxylation; carboxylation; desulphurization; denitration

check for updates

Citation: Lu, G.; Liao, H.; Zheng, X.; Chen, C.; Wang, W.; Xiao, X.; Qin, W. Effect of Hydroxylation and Carboxylation on the Catalytic Activity of Fe_2O_3/Graphene for Oxidative Desulfurization and Denitration. *Catalysts* **2022**, *12*, 1599. https://doi.org/10.3390/catal12121599

Academic Editors: Maria Luisa Di Gioia, Luísa Margarida Martins and Isidro M. Pastor

Received: 25 October 2022
Accepted: 30 November 2022
Published: 7 December 2022

1. Introduction

Environmental pollution caused by energy consumption is becoming more and more serious. When fossil fuels are burned, sulfur and nitrogen elements are mainly oxidized to SO_2 and NO [1]. Air pollution, acid rain, and the greenhouse effect, caused by harmful substances such as flue gas, sulfur oxides (mainly SO_2), and nitrogen oxides (mainly NO), are serious threats to human survival [2]. Therefore, it is urgent to strengthen the control of SO_2 and NO in flue gas. Many countries have issued strict standards to control the emission of SO_2 and NO below 50 ppm [3,4], which has prompted extensive efforts to develop effective technologies to reduce or remove these toxic gases [5]. The technologies that have been developed include wet flue gas desulfurization, dry sorbent injection, spray dryer absorption for desulfurization [6], low nitrogen oxide combustion technology, selective catalytic reduction (SCR), and selective noncatalytic reduction (SNCR) for denitration [7]. SCR technology was widely used in the flue gas treatment of coal-fired power plants, but its large scale and high cost limit its utilization in developing countries [8].

In order to make up for the deficiencies of current industrial technology, other methods are being studied, such as integrated oxidative desulfurization and denitration (ODSN) [9].

ODSN is expected to be a promising method for catalytic oxidization of SO_2 and NO in mild conditions, using a suitable catalyst for catalytic oxidation. Cu [9–11], Mn [12,13], Co [14], and Ce [15] are commonly used as catalysts by researchers. For example, Jie Ding et al. [16] used a Ce-Ti catalyst to catalyze the oxidation of NO_x and SO_2 by ozone, with the assistance of a glassy amino scrubber to remove sulfur and nitrogen. This process has no secondary pollution, but does have reduced waste production and a lower operating cost. Li et al. [17] used TiO_2/Cu_2O supported on activated carbon (AC) fiber as a photocatalyst to improve the adsorption ability of AC fiber for NO and SO_2. In addition, hematite (α-Fe_2O_3) is expected to be an ideal catalyst due to its low cost, good activity, and environmental performance. Alumina (Fe-Al) and H_2O_2 on the surface of hematite can achieve flue gas desulfurization and denitration simultaneously. Therefore, hematite-based catalysts have attracted more and more attention [18].

In the present report, the catalysts with strong adsorption capacity for SO_2 and NO and high selectivity for ODSN are still to be discovered. Carbon sorbent materials such as AC, graphite oxide (GO), single-walled carbon nanotubes (SWNTs), and graphene (G) are considered promising adsorbent materials for the selective removal of SO_2 and NO_x due to their high surface area and uniform pore size distribution. AC can effectively adsorb SO_2 and NO_x in flue gas at an aerobic low temperature, and its adsorption rate can reach over 99% [19]. Ammar et al. prepared metal oxide particles loaded on GO (PMO-Fe_3O_4 /rGO) as a heterogeneous catalyst/adsorbent, and hydrogen peroxide as an oxidant, achieving a denitration efficiency of 85.6% [20]. In the extractive catalytic oxidative desulfurization system, a sandwich-type polyoxometalate ($K_{10}[Co_4(H_2O)_2(PW_9O_{34})_2]_{10}$-($Co_4$-POM) was covalently immobilized on an amino-modified magnetic GO. When the catalyst was introduced into the reaction system, the oxidative desulfurization efficiency was 45.8%, and when acetonitrile was added as an extraction solvent, the sulfur was completely removed (100%) [21]. MoO_3 nanoparticles, supported on a carbon nanotubes catalyst, show high activity for oxidative desulfurization; the optimum sulfur removal efficiency was 96% [22]. Graphene has shown great potential in ODSN due to its unique single-atom-layer structure, high specific surface area, mechanical strength, fascinating thermal properties, and many surface-active sites [23–25]. Giulia Costamagna tailored the carbon surface with anchored iron nanoparticles and tested them for catalytic oxidative desulphurization of high sulfur content oil, proving the reliability of those materials as promising catalysts for upgrading sulfur-rich drop-in fuels [26]. Liao et al. used graphene to accelerate iron transport, significantly enhancing biological denitration and reducing intermediate accumulation [27]. Iron-based particles loaded on porous carbon material have attracted great attention due their low cost, non-toxicity, environmental protection, and excellent adsorption capacity to SO_2 and NO. However, the oxidation of carbon materials, such as hydroxylation and carboxylation, will inevitably occur in the oxidizing atmosphere [28], thus changing the adsorption and catalytic reaction capacity and reaction mechanisms of catalysts [29]. For example, high concentrations of oxygen and carbon dioxide would lead to the oxidation of AC [1], enhancing the NO and SO_2 adsorption capacity of AC, but reducing the efficiency of desulfurization and denitration [30]. A careful literature search revealed that the oxidation of carbon materials changes the catalytic activity. However, the mechanism of ODSN catalyst oxidation and its influence on the catalytic reaction has not yet been sufficiently studied. Accordingly, the present work is devoted to thoroughly investigating the adsorption and catalytic oxidation of SO_2 and NO on Fe_2O_3-loaded graphene models with carbon vacancy (G_{def}), hydroxyl (HyG), and carboxyl (CyG), by means of the DFT method. For the studied SO_2 and NO on Fe_2O_3/G_{def}, Fe_2O_3/HyG, and Fe_2O_3/CyG, the analyses of geometric structures, the adsorption energies, and the electronic properties were performed. Furthermore, the mechanism of the influence of H_2O_2 sprayed by the traditional hydrogen peroxide oxidative denitration technology on the catalytic desulfurization and denitration of Fe_2O_3/G_{def}, Fe_2O_3/HyG, and Fe_2O_3/CyG was studied. The research results reveal the variation characteristics of the catalyst performance, and have guiding significance for the development of new catalysts for ODSN.

2. Results and Discussion

2.1. Structure and Properties of Fe_2O_3/G_{def}, Fe_2O_3/HyG, and Fe_2O_3/CyG

Firstly, we compare and analyze the structural properties of Fe_2O_3/G_{def}, Fe_2O_3/HyG, and Fe_2O_3/CyG, as shown in Figure 1a. It can be inferred that after Fe_2O_3 is loaded on G_{def}, the Fe and O atoms are hybridized with the C atoms of G_{def}, the charge density is transferred from the Fe_2O_3 cluster to G_{def}, and the total Mulliken charge on the Fe_2O_3 cluster is 0.370. From Figure 1b, it can be concluded that for Fe_2O_3/HyG, the O atoms of Fe_2O_3 cannot bond with the C atoms of HyG, while Fe hybridizes with both the C atoms of HyG and the O atoms of hydroxyl (OH), resulting in the redistribution of charge density on atoms of Fe_2O_3/HyG. The total Mulliken charge of the Fe_2O_3 cluster loaded on HyG is −0.03. Compared with Fe_2O_3/G_{def}, the Fe_2O_3 cluster on HyG shows a weak negative charge. Figure 1c shows the stable configuration of Fe_2O_3/CyG, with only the Fe atom of the Fe_2O_3 cluster hybridizes with the C atom of CyG, and without direct interaction between the Fe_2O_3 cluster and the carboxyl (COOH) group. There was no hybridization between the metal oxides and carboxyl groups, which can be regarded as the common characteristics of Fe_2O_3 and CyG.

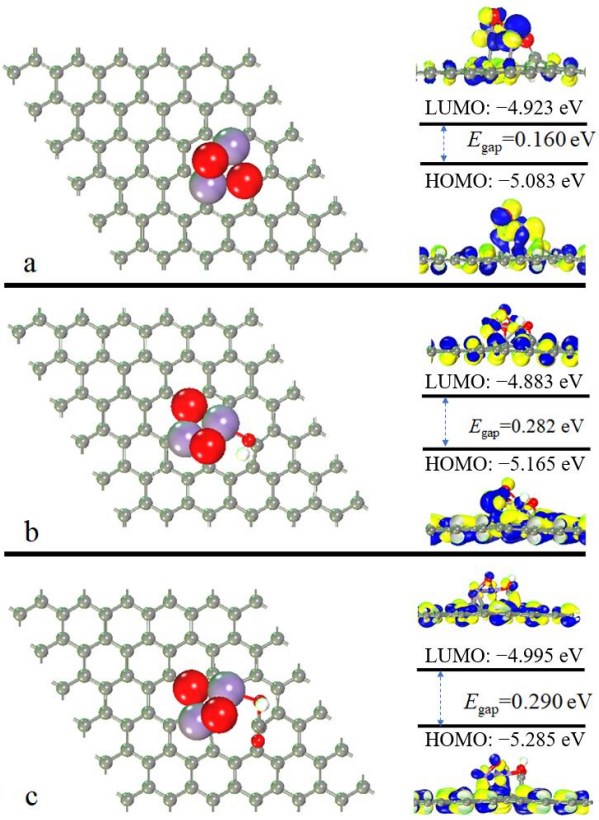

Figure 1. Stable configurations of (**a**) Fe_2O_3/G_{def}, (**b**) Fe_2O_3/HyG, and (**c**) Fe_2O_3/CyG with HOMO and LUMO. The C atom is gray, the O atom is red, the Fe atom is purple, and the H atom is white.

The stability of Fe_2O_3 on G_{def}, HyG, and CyG is evaluated by calculating the adsorption energy (E_{ads}) with Equation (13). Accordingly, the E_{ads} for Fe_2O_3/G_{def}, Fe_2O_3/HyG, and Fe_2O_3/CyG are −1.81 eV, −7.71 eV, and −9.61 eV, respectively. The results show that the presence of hydroxyl and carboxyl groups has a positive effect on the stability of the Fe_2O_3 cluster on the support.

To detail an understanding of the effect of the hydroxyl group and the carboxyl group on the electronic properties of the catalyst systems, we further analyzed the DOS for the Fe_2O_3 cluster supported on G_{def}, HyG, and CyG. As can be revealed in Figure 2, compared with the DOS of the pure Fe_2O_3 cluster, the DOS change of Fe_2O_3 loaded on G_{def}, HyG, and CyG indicated that there was a chemical interaction between Fe_2O_3 and G_{def}, HyG,

and CyG. Specifically, HyG and CyG promote the electron delocalization of Fe_2O_3 around the fermi level (E_f = 0.0 eV), which can improve the chemical activity of Fe_2O_3.

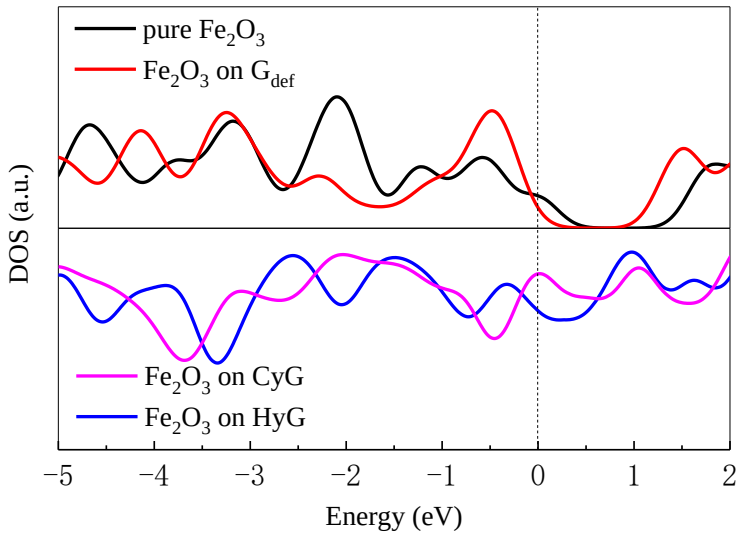

Figure 2. DOS for Fe_2O_3 before and after supported on G_{def}, HyG, and CyG. The vertical black dotted line indicates the Fermi level (EF = 0.000 eV).

2.2. NO and SO_2 Adsorption on Fe_2O_3/G_{def}, Fe_2O_3/HyG, and Fe_2O_3/CyG

The adsorption of NO and SO_2 on Fe_2O_3/G_{def} Fe_2O_3/HyG and Fe_2O_3/CyG is compared and discussed herein. Figure 3a–c depict the optimized models, which are the stable adsorption configurations of NO on the surface of Fe_2O_3/G_{def}, Fe_2O_3/HyG, and Fe_2O_3/CyG, respectively. The N atom interacts with the Fe atom chemically, and the bond lengths are 1.711 Å, 1.652 Å, and 1.675 Å, respectively. The electronic interaction between NO and the catalyst leads to charge rearrangement, and the bond lengths of N-O become 1.180 Å, 1.187 Å, and 1.179 Å, respectively, which are larger than the bond lengths of free NO molecule (1.151 Å). For the configurations of SO_2 adsorption on Fe_2O_3/G_{def}, Fe_2O_3/HyG, and Fe_2O_3/CyG, as shown in Figure 3d–f, the S atom was adsorbed by the Fe atom to form an S-Fe bond, with bond lengths of 2.222 Å, 2.211 Å, and 2.641 Å, respectively. After adsorption, the bond length and bond angle of SO_2 changed slightly, while the charge density of SO_2 increased by 0.167, 0.197, and 0.143 on Fe_2O_3/G_{def}, Fe_2O_3/HyG, and Fe_2O_3/CyG, respectively.

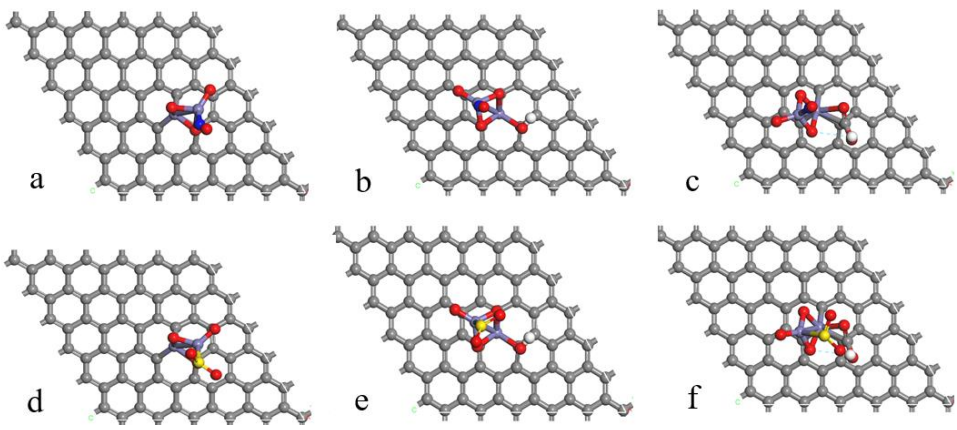

Figure 3. (**a**–**c**) Stable configurations of NO adsorption on Fe_2O_3/G_{def}, Fe_2O_3/HyG, and Fe_2O_3/CyG. (**d**–**f**) Stable configurations of SO_2 adsorption on Fe_2O_3/G_{def}, Fe_2O_3/HyG, and Fe_2O_3/CyG. The C atom is gray, the O atom is red, the Fe atom is purple, the H atom is white, the N atom is blue, and the S atom is yellow.

The E_{ads} for NO [and SO_2] on Fe_2O_3/G_{def}, Fe_2O_3/HyG, and Fe_2O_3/CyG are calculated by the Equation (13). As shown in Table 1, E_{ads} are all negative, which indicates that the adsorption of NO and SO_2 on Fe_2O_3/G_{def}, Fe_2O_3/HyG, and Fe_2O_3/CyG are exothermic processes. Hydroxylation and carboxylation decreased the E_{ads} of NO on surfaces and increased the E_{ads} of SO_2 on surfaces. However, the E_{ads} of SO_2 on surfaces was much less than that of NO on these catalysts. The interaction between NO and the surfaces are stronger than those of SO_2.

Table 1. E_{ads} for NO [and SO_2] adsorption on Fe_2O_3/G_{def}, Fe_2O_3/HyG, and Fe_2O_3/CyG.

	Adsorption Energy (eV)
NO-Fe_2O_3/G_{def}	−2.20
NO-Fe_2O_3/HyG	−1.22
NO-Fe_2O_3/CyG	−1.06
SO_2-Fe_2O_3/G_{def}	−0.16
SO_2-Fe_2O_3/HyG	−0.33
SO_2-Fe_2O_3/CyG	−0.41

We further researched the adsorption of NO and SO_2 on Fe_2O_3/G_{def}, Fe_2O_3/HyG, and Fe_2O_3/CyG. Figure 4 displays the DOS of N_{2p}, Fe_{3d}, and SO_2 on Fe_2O_3/G_{def}, Fe_2O_3/HyG, and Fe_2O_3/CyG. The comparison before and after adsorption revealed that N_{2p}-DOS and Fe_{3d}-DOS change significantly around the Fermi level. N_{2p}-DOS and Fe_{3d}-DOS split to form bonding and antibonding orbitals, and the orbital energies overlap well, further confirming that NO is chemisorbed on Fe_2O_3/G_{def} and Fe_2O_3/HyG. A Mulliken charge analysis revealed that the total charges of the adsorbed NO on Fe_2O_3/G_{def}, Fe_2O_3/HyG, and Fe_2O_3/CyG were −0.050, 0.032, and 0.023, respectively. Hydroxylation and carboxylation slightly modulated the charge population between NO and the catalyst; that is, the oxidation of graphene will affect the adsorption of NO. For the adsorption of SO_2 on Fe_2O_3/G_{def}, Fe_2O_3/HyG, and Fe_2O_3/CyG, the SO_2-DOS shifts to the left, indicating that part of the charge is transferred to SO_2 after adsorption. However, the DOS only shows a left shift, without any splitting after SO_2 adsorption on Fe_2O_3/HyG and Fe_2O_3/CyG, which implies that only physical adsorption occurs for SO_2-Fe_2O_3/HyG and SO_2-Fe_2O_3/CyG.

2.3. Catalytic Oxidation of SO_2 and NO on Fe_2O_3/G_{def}, Fe_2O_3/HyG, and Fe_2O_3/CyG

In this section, the catalytic oxidation reaction mechanism of desulfurization and denitration was studied. The reaction mechanism of NO oxidation via hydroxyl radical ·OH in the gas phase is as follows:

$$\cdot\mathrm{OH} + \mathrm{NO} \rightarrow \mathrm{HNO_2} \qquad \Delta_r H = -2.15\ \mathrm{eV} \tag{1}$$

$$\mathrm{HNO_2} + \cdot\mathrm{OH} \rightarrow \mathrm{H_2NO_3} \qquad \Delta_r H = -0.31\ \mathrm{eV} \tag{2}$$

The corresponding rate Equation:

$$\mathrm{r} = \frac{k\mathrm{T}}{h}\mathrm{Exp}\left(\frac{-0.21\ \mathrm{eV} \times 6.02 \times 10^{23} \times 1.6 \times 10^{-19}}{R}\right) \tag{3}$$

The reaction mechanism of SO_2 oxidation via hydroxyl radical ·OH in the gas phase is as follows:

$$\cdot\mathrm{OH} + \mathrm{SO_2} \rightarrow \mathrm{HSO_3} \qquad \Delta_r H = -1.54\ \mathrm{eV} \tag{4}$$

$$\mathrm{HSO_3} + \cdot\mathrm{OH} \rightarrow \mathrm{H_2SO_4} \qquad \Delta_r H = -3.77\ \mathrm{eV} \tag{5}$$

The thermal effect of SO_2 oxidation via ·OH was more obvious than that of NO oxidation. NO and SO_2 oxidation via ·OH is thermodynamic feasible, and the process is exothermic.

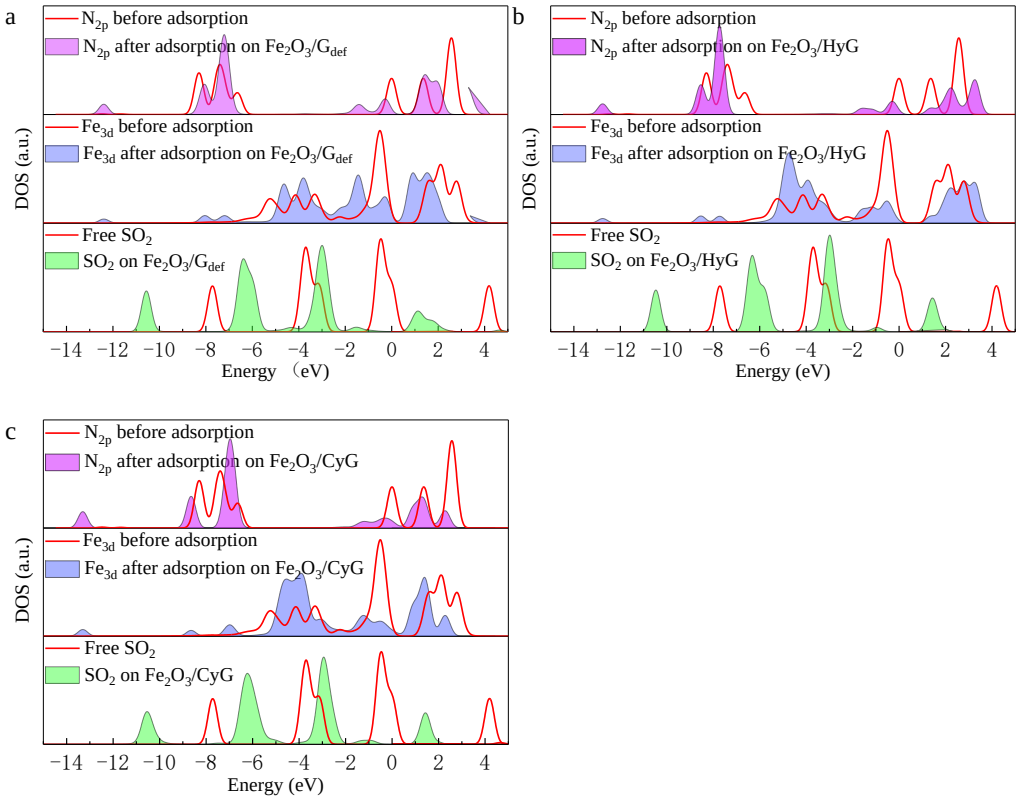

Figure 4. N_{2p}-DOS, SO_2-DOS, and Fe_{3d}-DOS on (**a**) Fe_2O_3/G_{def}, (**b**) Fe_2O_3/HyG, and(**c**) Fe_2O_3/CyG.

The traditional hydrogen peroxide oxidation denitration technology is to spray H_2O_2 at the flue gas at above 400 °C. H_2O_2 decomposes into the free hydroxyl radical ·OH, which oxidizes NO into NO_2, and then the alkaline solution is used to absorb the generated NO_2. However, H_2O_2 also generates radical ·OOH, which cannot oxidize NO, but combines with ·OH to generate H_2O and O_2. Moreover, the decomposition reaction of H_2O_2 into ·OH in the gas phase is thermodynamically unfeasible. Therefore, we discussed the adsorption of H_2O_2 on Fe_2O_3/G_{def}, Fe_2O_3/HyG, and Fe_2O_3/CyG.

H_2O_2 is physically adsorbed on Fe_2O_3/G_{def}, Fe_2O_3/HyG, and Fe_2O_3/CyG, forming a stable adsorption configuration with two hydrogen bonds, as shown in Figure 5. It can be seen that H_2O_2 adsorbed on the catalyst surface site without decomposition. After H_2O_2 is adsorbed on the surface of the Fe_2O_3/G_{def}, the O-O bond length was 1.438 Å, which was close to that (1.439 Å) of the pure H_2O_2. The two H atoms of H_2O_2 and the two O atoms of Fe_2O_3 form hydrogen bonds with lengths of 2.325 Å and 2.466 Å, respectively. While H_2O_2 is adsorbed on the surface of Fe_2O_3/HyG, the O-O bond length is 1.467 Å, which is longer than that of pure H_2O_2. One H of H_2O_2 adsorbed on Fe_2O_3/HyG forms a hydrogen bond (1.708 Å) with one O atom of Fe_2O_3, while another O atom of H_2O_2 forms another hydrogen bond (1.724 Å) with an H atom of hydroxyl. For the stable configuration of H_2O_2-Fe_2O_3/CyG, the O-O has a bond length of H_2O_2 1.437 Å. One H atom of H_2O_2 adsorbed on Fe_2O_3/ CyG forms a hydrogen bond (1.708 Å) with one O atom of Fe_2O_3, and another O atom of H_2O_2 forms a hydrogen bond (1.641 Å) with an H atom of the carboxyl.

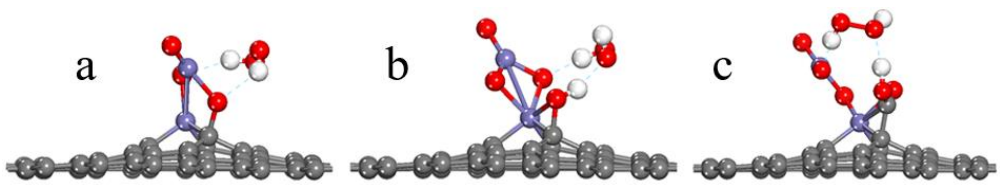

Figure 5. Stable configuration of H_2O_2 adsorption on (**a**) Fe_2O_3/G_{def}, (**b**) Fe_2O_3/HyG, and (**c**) Fe_2O_3/CyG. The C atom is gray, the O atom is red, the Fe atom is purple, and the H atom is white.

Similar to Equation (13), the E_{ads} of H_2O_2 on Fe_2O_3/G_{def}, Fe_2O_3/HyG, and Fe_2O_3/CyG can be calculated as −0.35 eV, −1.27 eV, and −2.29 eV, respectively. Hydroxylation and carboxylation significantly enhance the interaction between H_2O_2 and the catalysts.

In order to explain the adsorption characteristics of H_2O_2 more accurately, we analyzed the electron characteristics of H_2O_2 adsorbed on the catalyst surface. Figure 6 shows the DOS of H_2O_2 adsorption on Fe_2O_3/G_{def}, Fe_2O_3/HyG, and Fe_2O_3/CyG. Before adsorption, the outer orbital π* of H_2O_2 was half-filled. After adsorption, H_2O_2 accepted electron transferring by Fe_2O_3/G_{def}, Fe_2O_3/HyG, and Fe_2O_3/CyG. The outer orbitals were fully filled, and the DOS of H_2O_2 shifted to the left. The DOS of H_2O_2 adsorbed on Fe_2O_3/G_{def} and H_2O_2-Fe_2O_3/HyG shifted to the left by approximately 1 eV, while the DOS of H_2O_2 adsorbed on Fe_2O_3/CyG shifted to the left by approximately 2 eV. Hydroxylation and carboxylation can significantly change the DOS of H_2O_2. The carboxylation enhances the adsorption stability of H_2O_2 on the catalyst surface, which corresponds to the adsorption energy calculated above.

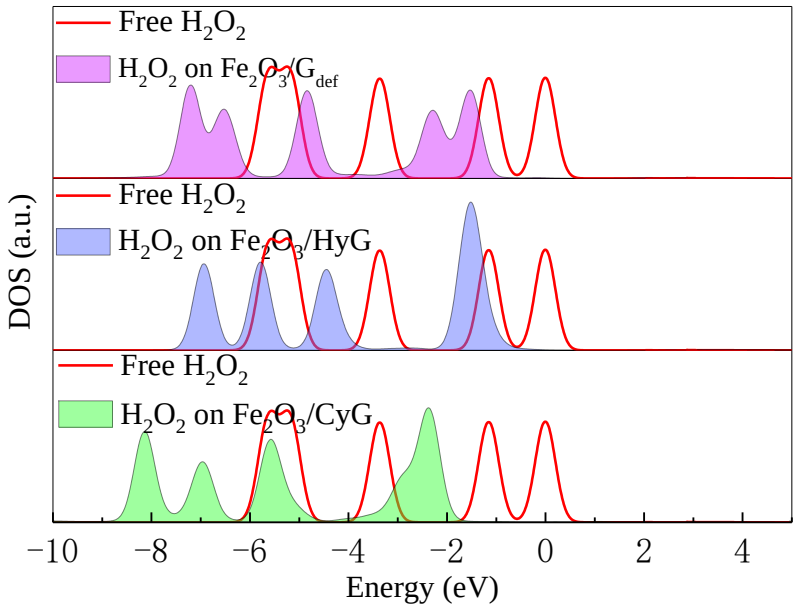

Figure 6. DOS for the free H_2O_2, the H_2O_2 on Fe_2O_3/G_{def}, the H_2O_2 on Fe_2O_3/HyG, and the H_2O_2 on Fe_2O_3/CyG.

Although the physical adsorption of H_2O_2 on Fe_2O_3/HyG and Fe_2O_3/CyG cannot lead to the generation of ·OH directly; it adjusts the extent of the reaction balance and promotes the oxidation of NO and SO_2. It was found that Fe_2O_3/G_{def} catalyzes the oxidation of NO by H_2O_2 to form the adsorbed HNO_2, and releases an ·OH group to the gas phase for further oxidation as:

$$NO + H_2O_2\text{-}Fe_2O_3/G_{def} \rightarrow HNO_2\text{-}Fe_2O_3/G_{def} + \cdot OH \quad (6)$$

$$\cdot OH + NO \rightarrow HNO_2 \quad (7)$$

$$HNO_2 + \cdot OH \rightarrow H_2NO_3 \quad (8)$$

As shown in Figure 7a, differing from the reaction on Fe_2O_3/G_{def}, H_2O_2 oxidizes NO into free nitrous acid molecules on Fe_2O_3/HyG and Fe_2O_3/CyG. Hydroxylation and carboxylation of Fe_2O_3/HyG and Fe_2O_3/CyG can catalyze H_2O_2 to oxidize NO to HNO_2 in one step, as:

$$NO + H_2O_2\text{-}Fe_2O_3/HyG \rightarrow H_2NO_3 + Fe_2O_3/HyG \quad (9)$$

$$NO + H_2O_2\text{-}Fe_2O_3/CyG \rightarrow H_2NO_3 + Fe_2O_3/CyG \quad (10)$$

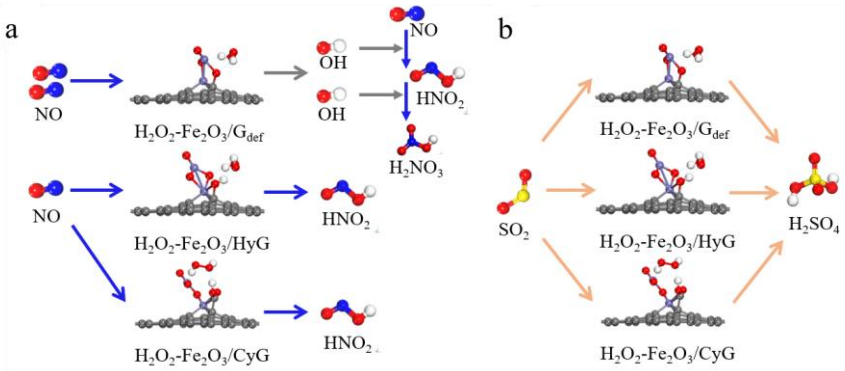

Figure 7. Schematic diagram of the mechanism of (**a**) NO and (**b**) SO_2 oxidation on H_2O_2-Fe_2O_3/G_{def}, H_2O_2-Fe_2O_3/HyG, and H_2O_2-Fe_2O_3/CyG. The C atom is gray, the O atom is red, the Fe atom is purple, the H atom is white, the N atom is blue, and the S atom is yellow.

Similarly, as shown in Figure 7b, the surface adsorption of H_2O_2 on Fe_2O_3/G_{def}, Fe_2O_3/HyG, and Fe_2O_3/CyG cannot directly decompose into ·OH, but adjusts the extent of the reaction balance to promote the oxidation reaction of SO_2. $Fe_2O_3/G_{def,}$ Fe_2O_3/HyG, and Fe_2O_3/CyG can directly adsorb H_2O_2 and oxidize SO_2 into sulfuric acid molecules on the surface. Therefore, the mechanism of Fe_2O_3/G_{def}, Fe_2O_3/HyG, and Fe_2O_3/CyG catalyzing H_2O_2 to oxidize SO_2 is as follows:

$$H_2O_2 \overset{\text{Cat.}}{\rightarrow} H_2O_2\text{-Cat.} \tag{11}$$

$$SO_2 + H_2O_2\text{-Cat.} \rightarrow H_2SO_4 + \text{Cat.} \tag{12}$$

where Cat. is the catalysts (Fe_2O_3/G_{def}, Fe_2O_3/HyG, and Fe_2O_3/CyG).

3. Model and Methods

The DFT [31] calculations were carried out using Dmol^3 module in the Materials Studio software package, with Generalized Gradient Approximation (GGA) and Perdew-Burke-Ernzerhof (PBE) functional [32] for exchange and correlation potentials. Double numerical basis sets, plus polarization function (DNP), were used for atomic basis functions. The DFT semi-core pseudopots method was used for core treatment. The plane wave cutoff energy was set to 600 eV. The self-consistent accuracy was set to 2×10^{-5} eV/atom. A maximum force tolerance of 0.002 Ha/Å was applied. Following previous work [33,34], the 6×6 graphene flake, composed of 72 carbon atoms and a vacuum layer with a thickness of 15 Å, was established. One C atom of the graphene sheet was removed in order to obtain the C-defect graphene (G_{def}) by geometric optimization. The hydroxyl and carboxyl groups were grafted onto the defect sites of G_{def} to obtain the configurations of HyG and CyG, respectively. Three stable catalyst models of Fe_2O_3/G_{def}, Fe_2O_3/HyG, and Fe_2O_3/CyG were obtained by loading the Fe_2O_3 cluster on the modified graphene surfaces.

The adsorption energy (E_{ads}) was calculated as:

$$E_{ads} = E_{\text{adsorbate,surface}} - E_{\text{surface}} - E_{\text{adsorbate}} \tag{13}$$

where $E_{\text{adsorbate,surface}}$, E_{surface}, and $E_{\text{adsorbate}}$ represent the total energy of the surface slabs with adsorbates, the bare slabs, and adsorbates, respectively. A negative E_{ads} value indicates that the adsorption process is exothermic, whereas a positive value indicates an endothermic process. The adsorption stability of Fe_2O_3 on G_{def}, HyG, and CyG, as well as the NO and SO_2 on Fe_2O_3/G_{def}, Fe_2O_3/HyG, and Fe_2O_3/CyG, can be evaluated by calculating the E_{ads}.

4. Conclusions

In the current study, the effects of hydroxylation and carboxylation on the catalytic activity of Fe_2O_3/graphene for ODSN are investigated using DFT calculations. Adsorption energies, charge transfer analyses, and DOS calculations were performed for NO, SO_2, H_2O_2, and Fe_2O_3/graphene configurations. The hydroxyl group and carboxyl group permitted more stable adsorption of the Fe_2O_3 clusters on graphene and promoted the electron delocalization of Fe_2O_3 around the Fermi level, evidencing the enhanced chemical activity of Fe_2O_3. Hydroxylation and carboxylation improved the adsorption of SO_2 and H_2O_2 on Fe_2O_3/graphene, and maintained the preferable adsorption stability of NO. The DOS of N_{2p}, Fe_{3d}, and SO_2 on Fe_2O_3/G_{def}, Fe_2O_3/HyG, and Fe_2O_3/CyG verified that NO was chemisorbed on Fe_2O_3/G_{def} and Fe_2O_3/HyG, while only physical adsorption occurred for the SO_2-Fe_2O_3/HyG and SO_2-Fe_2O_3/CyG. Fe_2O_3/G_{def} catalyzed the oxidation of NO by H_2O_2 to form the adsorbed HNO_2 and to release a ·OH group to the gas phase. H_2O_2 oxidizes NO into free nitrous acid molecules on the surface of Fe_2O_3/HyG, and Fe_2O_3/CyG via a one-step reaction mechanism. Similarly, Fe_2O_3/G_{def}, Fe_2O_3/HyG, and Fe_2O_3/CyG can directly adsorb H_2O_2 and oxidize SO_2 into sulfuric acid molecules on the surface. The results provide a fundamental understanding of catalyst oxidative denaturation on catalytic denitration and desulfurization reactions.

Author Contributions: Writing—original draft preparation, G.L.; writing—review and editing, H.L.; visualization, X.Z.; supervision, C.C.; project administration, W.W.; funding acquisition, X.X. and W.Q. All authors have read and agreed to the published version of the manuscript.

Funding: This work was funded by Tianjin Guoneng Jinneng Binhai Thermal Power Co., Ltd. #2 Furnace Temperature Field Visualization and Combustion Optimization Research and Application Technology Innovation Project (JBRD2022037).

Data Availability Statement: All data that support the plots and other findings within this paper are available from the corresponding authors on reasonable request.

Conflicts of Interest: The authors declare no conflict of interest.

References

1. Ma, S.-C.; Yao, J.-J.; Gao, L.; Ma, X.-Y.; Zhao, Y. Experimental study on removals of SO_2 and NO_x using adsorption of activated carbon/microwave desorption. *J. Air Waste Manag. Assoc.* **2012**, *62*, 1012–1021. [CrossRef] [PubMed]
2. Shah, M.P.; Rodriguez-Couto, S.; Kapoor, R. *Development in Wastewater Treatment Research and Processes*, 1st ed.; Elsevier: Amsterdam, The Netherlands, 2022; pp. 61–106.
3. De Lima, F.M.; De Andrade Borges, T.; Braga, R.M.; De Araújo Melo, D.M.; Martinelli, A.E. Sulfur removal from model fuel by Zn impregnated retorted shale and with assistance of design of experiments. *Environ. Sci. Pollut. Res.* **2018**, *25*, 13760–13774. [CrossRef] [PubMed]
4. University College London. China Is on Track to Meet Its Emissions Goals for 2020. Available online: www.sciencedaily.com/releases/2019/10/191007113327.htm (accessed on 24 October 2022).
5. Song, Y.; Zhang, Y.; Wu, Q.; Kang, D.; Guo, S.; Zhou, H. Experimental Study on the Desulfurization, Denitration, and Dust Removal Characteristics of Ceramic Fiber Filter Tubes. *Energy Fuels* **2022**, *36*, 3715–3726. [CrossRef]
6. Koech, L.; Rutto, H.; Lerotholi, L.; Everson, R.C.; Neomagus, H.; Branken, D.; Moganelwa, A. Spray drying absorption for desulphurization: A review of recent developments. *Clean Technol. Environ. Policy* **2021**, *23*, 1665–1686. [CrossRef]
7. Gholami, F.; Tomas, M.; Gholami, Z.; Vakili, M. Technologies for the nitrogen oxides reduction from flue gas: A review. *Sci. Total Environ.* **2020**, *714*, 136712. [CrossRef]
8. Prabhu, S.S. A Review on Selective Catalytic Reduction (SCR)-A Promising Technology to mitigate NO_x of Modern Automobiles. *Int. J. Appl. Eng. Res.* **2018**, *13*, 5–9.
9. Pham, A.N.; Xing, G.; Miller, C.J.; Waite, T.D. Fenton-like copper redox chemistry revisited: Hydrogen peroxide and superoxide mediation of copper-catalyzed oxidant production. *J. Catal.* **2013**, *301*, 54–64. [CrossRef]
10. Xiao, F.S.; Sun, J.; Meng, X.; Yu, R.; Yuan, H.; Xu, J.; Song, T.; Jiang, D.; Xu, R. Synthesis and Structure of Copper Hydroxyphosphate and Its High Catalytic Activity in Hydroxylation of Phenol by H_2O_2. *J. Catal.* **2001**, *199*, 155–346. [CrossRef]
11. Subbaramaiah, V.; Srivastava, V.C.; Mall, I.D. Mall, Catalytic Activity of Cu/SBA-15 for Peroxidation of Pyridine Bearing Wastewater at Atmospheric Condition. *Aiche J.* **2013**, *59*, 2577–2586. [CrossRef]
12. Han, Y.F.; Chen, F.; Ramesh, K.; Zhong, Z.; Widjaja, E.; Chen, L. Preparation of nanosized Mn_3O_4/SBA-15 catalyst for complete oxidation of low concentration EtOH in aqueous solution with H_2O_2. *Appl. Catal. B Environ.* **2007**, *76*, 227–234. [CrossRef]

13. Sriskandakumar, T.; Opembe, N.; Chen, C.H.; Morey, A.; King'ondu, C.; Suib, S.L. Green Decomposition of Organic Dyes Using Octahedral Molecular Sieve Manganese Oxide Catalysts. *J. Phys. Chem. A* **2009**, *113*, 1523–1530. [CrossRef]
14. Valdés-Solís, T.; Valle-Vigón, P.; Sevilla, M.; Fuertes, A.B. Encapsulation of nanosized catalysts in the hollow core of a mesoporous carbon capsule. *J. Catal.* **2007**, *251*, 239–243. [CrossRef]
15. Heckert, E.G.; Seal, S.; Self, W.T. Fenton-Like Reaction Catalyzed by the Rare Earth Inner Transition Metal Cerium. *Environ. Sci. Technol.* **2008**, *42*, 5014–5019. [CrossRef]
16. Ding, J.; Zhong, Q.; Zhang, S. Simultaneous desulfurization and denitrification of flue gas by catalytic ozonation over Ce-Ti catalyst. *Fuel Process. Technol.* **2014**, *128*, 449–455. [CrossRef]
17. Li, C.-J.; Zhao, R.; Peng, M.-Q.; Hao, L.; Gang, Y.; Dong-Sheng, X. Study on desulfurization and denitrification by modified activated carbon fibers with visible-light photocatalysis. *J. Fuel Chem. Technol.* **2015**, *43*, 1516–1522. [CrossRef]
18. Song, Z.; Wang, B.; Yu, J.; Ma, C.; Zhou, C.; Chen, T.; Yan, Q.; Wang, K.; Sun, L. Density functional study on the heterogeneous oxidation of NO over α-Fe_2O_3 catalyst by H_2O_2: Effect of oxygen vacancy. *Appl. Surf. Sci.* **2017**, *413*, 292–301. [CrossRef]
19. Wang, S.; Xu, S.; Gao, S.; Xiao, P.; Jiang, M.; Zhao, H.; Bin Huang, B.; Liu, L.; Niu, H.; Wang, J.; et al. Simultaneous removal of SO_2 and NO_x from flue gas by low-temperature adsorption over activated carbon. *Sci. Rep.* **2021**, *11*, 11003. [CrossRef]
20. Ammar, S.H.; Kareem, Y.S.; Mohammed, M.S. Catalytic-oxidative/adsorptive denitrogenation of model hydrocarbon fuels under ultrasonic field using magnetic reduced graphene oxide-based phosphomolybdic acid (PMo-Fe_3O_4/rGO). *Ultrason. Sonochem.* **2020**, *64*, 105050. [CrossRef]
21. Nejati, F.M.; Shahhosseini, S.; Rezaee, M. Cobalt-based sandwich-type polyoxometalate supported on amino-silane decorated magnetic graphene oxide: A recoverable catalyst for extractive-catalytic oxidative desulfurization of model oil. *J. Environ. Chem. Eng.* **2022**, *10*, 107949. [CrossRef]
22. Alwan, H.H. Oxidative desulfurization of a model fuel using MoO_3 nanoparticles supported on carbon nanotubes catalyst: Examine most significance variables, optimization, kinetics and thermodynamics study. *South Afr. J. Chem. Eng.* **2022**, *40*, 230–239. [CrossRef]
23. Li, T.; Yin, W.; Gao, S.; Sun, Y.; Xu, P.; Wu, S.; Kong, H.; Yang, G.; Wei, G. The Combination of Two-Dimensional Nanomaterials with Metal Oxide Nanoparticles for Gas Sensors: A Review. *Nanomaterials* **2022**, *12*, 982. [CrossRef] [PubMed]
24. Ibrahim, M.A.A.; Mahmoud, A.H.M.; Soliman, K.A.; Mekhemer, G.A.H.; Ahmed, M.N.; Shawky, A.M.; Abourehab, M.A.S.; Elkaeed, E.B.; Soliman, M.E.S.; Moussa, N.A.M. Borophene and Pristine Graphene 2D Sheets as Potential Surfaces for the Adsorption of Electron-Rich and Electron-Deficient π-Systems: A Comparative DFT Study. *Nanomaterials* **2022**, *12*, 1028. [PubMed]
25. Betiha, M.A.; Rabie, A.M.; Ahmed, H.S.; Abdelrahman, A.A.; El-Shahat, M.F. Oxidative desulfurization using graphene and its composites for fuel containing thiophene and its derivatives: An update review. *Egypt. J. Pet.* **2018**, *27*, 715–730. [CrossRef]
26. Tamborrino, V.; Costamagna, G.; Bartoli, M.; Rovere, M.; Jagdale, P.; Lavagna, L.; Ginepro, M.; Tagliaferro, A. Catalytic oxidative desulphurization of pyrolytic oils to fuels over different waste derived carbon-based catalysts. *Fuel* **2021**, *296*, 120693. [CrossRef]
27. Liao, Y.; Li, S.; Zhu, X.; Dang, Z.; Tang, S.; Ji, G. The promotion and inhibition effect of graphene oxide on the process of microbial denitrification at low temperature. *Bioresour. Technol.* **2021**, *340*, 125636. [CrossRef]
28. Gao, Y.; Wang, Q.; Ji, G.; Li, A. Degradation of antibiotic pollutants by persulfate activated with various carbon materials. *Chem. Eng. J.* **2022**, *429*, 132387. [CrossRef]
29. Chamoli, P.; Banerjee, S.; Raina, K.K.; Kar, K.K. *Handbook of Nanocomposite Supercapacitor Materials I*, 1st ed.; Springer: Cham, Switzerland, 2020; pp. 155–177.
30. Ma, S.-C.; Gao, L.; Ma, J.-X.; Jin, X.; Yao, J.-J.; Zhao, Y. Advances on simultaneous desulfurization and denitrification using activated carbon irradiated by microwaves. *Environ. Technol.* **2012**, *33*, 1225–1230. [CrossRef]
31. Inada, Y.; Orita, H. Efficiency of numerical basis sets for predicting the binding energies of hydrogen bonded complexes: Evidence of small basis set superposition error compared to Gaussian basis sets. *J. Comput. Chem.* **2008**, *29*, 225–232. [CrossRef]
32. Perdew, J.P.; Burke, K.; Ernzerhof, M. Generalized Gradient Approximation Made Simple. *Phys. Rev. Lett.* **1996**, *77*, 3865–3868. [CrossRef]
33. Qin, W.; Li, X.; Bian, W.-W.; Fan, X.-J.; Qi, J.-Y. Density functional theory calculations and molecular dynamics simulations of the adsorption of biomolecules on graphene surfaces. *Biomaterials* **2010**, *31*, 1007–1016. [CrossRef]
34. Qin, W.; Li, X. A Theoretical Study on the Catalytic Synergetic Effects of Pt/Graphene Nanocomposites. *J. Phys. Chem. C* **2010**, *114*, 19009–19015. [CrossRef]